


Article

The Feasibility of Shadowed Image Restoration Using the Synthetic Aperture Focusing Technique

Kuo-Yuan Huang ¹, Chih-Hsiung Chang ^{2,*}, Young-Fo Chang ³, Jia-Wei Liu ⁴ and Jer-Wei Chang ⁵

¹ Department of Orthopedics, National Cheng Kung University Hospital, College of Medicine, National Cheng Kung University, Tainan 70403, Taiwan

² Department of Biomechatronic Engineering, Research Center for Automation, National Chiayi University, Chiayi 60004, Taiwan

³ Institute of Seismology, National Chung Cheng University, Chiayi 62102, Taiwan

⁴ Green Energy and Environment Research Laboratories, Industrial Technology Research Institute, Hsinchu 31040, Taiwan

⁵ Department of Computer Science and Information Engineering, National Chiayi University, Chiayi 60004, Taiwan

* Correspondence: charles@mail.ncyu.edu.tw; Tel.: +886-5-226-3411

Featured Application: At present, there is no relevant research which explores possible lesions in ultrasound images that may exist in acoustic shadow; only a differential diagnosis can be made. This current work addresses the use of a reliable posterior restoration algorithm for possible acoustic shadowed lesions. Our results reveal the potential for a SAFT-based restorative application that may provide diagnostic information in medical sonography.



Citation: Huang, K.-Y.; Chang, C.-H.; Chang, Y.-F.; Liu, J.-W.; Chang, J.-W. The Feasibility of Shadowed Image Restoration Using the Synthetic Aperture Focusing Technique. *Appl. Sci.* **2022**, *12*, 9297. <https://doi.org/10.3390/app12189297>

Academic Editors: Cecilia Di Ruberto, Andrea Loddo, Lorenzo Putzu, Alessandro Stefano and Albert Comelli

Received: 21 August 2022

Accepted: 13 September 2022

Published: 16 September 2022

Publisher's Note: MDPI stays neutral with regard to jurisdictional claims in published maps and institutional affiliations.



Copyright: © 2022 by the authors. Licensee MDPI, Basel, Switzerland. This article is an open access article distributed under the terms and conditions of the Creative Commons Attribution (CC BY) license (<https://creativecommons.org/licenses/by/4.0/>).

Abstract: The phenomenon of acoustic shadowing on ultrasonography is characterized by an echo signal void behind structures that strongly absorb or reflect ultrasonic energy. In medical ultrasonography, once the ultrasound energy is shielded, acoustic shadowing makes it difficult to create an image, leading to misinterpretations and obscure diagnoses. Hence, instead of dealing with the defocused problem encountered in an ultrasound scan (US), this current research focuses on revealing the existence of an acoustically shadowed target (or a potential lesion) using a well-known restoration algorithm, i.e., the synthetic aperture focusing technique (SAFT). To demonstrate the effects of an acoustic shadow on an ultrasound scan (US), a forward model study is carried out. In laboratory manipulations, a purposely designed physical model is created and then scanned using B-mode and pitch/catch arrangements to carry out shadowed and shadow-free scans in a water tank. Thereafter, making use of a delay-and-sum (DAS) operation, the echo signals are processed by the synthetic aperture focusing technique (SAFT) to perform image restoration. The results of the restoration process show that the SAFT algorithm performs well with respect to directional shadowing. Once the target or lesion is positioned in a total anechoic zone, or even in a multi-channel scan, it will fail.

Keywords: ultrasound; acoustic shadow; image restoration; SAFT

1. Introduction

The advantageous properties of ultrasound scanning (US), such as non-invasiveness and non-radiation, are widely used in medical diagnosis [1–3]. US uses the interaction of high-frequency acoustic energy in a specimen to produce an original image that reveals tissues inside the human body. High-frequency (1 to 20 MHz) sound energy is transmitted into a specimen by an ultrasound machine in the form of multiple pulses, and the echoes are relayed on a monitor and form a two-dimensional image. However, the US still suffers from limitations in resolution, contrast, and signal-to-noise ratio (SNR), and is not free from artefacts [4]. Acoustic shadowing, a feature of ultrasound images, is one of the artefacts inherent in US imaging.

Acoustic shadowing is detected as an ultrasonic manifestation. Occurrences of anechoic zones caused by acoustic shadowing are devoid of echo and fail to render reliable images in US [3,5]. In response to acoustic shadowing, the anechoic zone displays as a dark area, e.g., due to the echogenic appearance of tissue posterior to kidney stones, gallstones, benign or malignant tumors, foreign bodies, complex sclerosing lesions, postoperative scars, fibrous or dense breast tissue, etc. [6–9]. Hence, in a traditional sonographic examination, acoustic shadowing is often used to explore possible relevant differential diagnoses rather than the further use of ultrasound to diagnose the shadowed lesions [10].

In medical sonography, a shadowed tissue induced by acoustic shadowing cannot be revealed by increasing the power or gain of the ultrasound machine. However, due to the directionality of acoustic shadowing and the acoustic radiation (beam) pattern, a shadowed target that is echo-free at a specific scan position can be echoed in other scan positions in a multi-channel scan [11,12]. Hence, it is critical and worthwhile for us to overcome the artefacts resulting from acoustic shadowing that degrade the attainable ultrasonic image. Typically, a posterior restoration process is employed to reconstruct the original image from observations.

Nowadays, restoration techniques are significantly advanced, owing to the development of digital processes [13,14]. With the heuristic principle of signal superposition via constructive interference, the synthetic aperture focusing technique (SAFT) algorithm allows each point within the target to be focused upon by mathematically simulating the action of a lens specifically formed for imaging the target inside the structure. The efficiencies and easy manipulation make SAFT one of the most popular processing technologies used to improve image quality and maximize the resolution from acquired echo signals. SAFT is proposed to facilitate the original image restoration by trying to “undo” the effects of acoustic shadowing on an ultrasonic image [15,16].

The acoustic shadowing encountered in the sonographic examination is often used to explore possible relevant differential diagnoses, rather than to reveal the shadowed lesions [7,17]. In this study, a forward model study is carried out to demonstrate the phenomenon of acoustic shadowing in US and to perform data acquisition. In the posterior stage of image restoration, the acquired data are then processed by SAFT. It is hoped that a potential target hidden under acoustic shadowing can be revealed from restored images. The remainder of this article is therefore organized as follows. First, the laboratory manipulation designed to facilitate the acoustic shadowing experiment is introduced. Subsequently, the theoretical background of SAFT, which is used to perform shadowed image restoration, is briefly described, and the results of laboratory work are presented. Finally, the applications and limitations of the restoration algorithm are addressed in the discussions and conclusions.

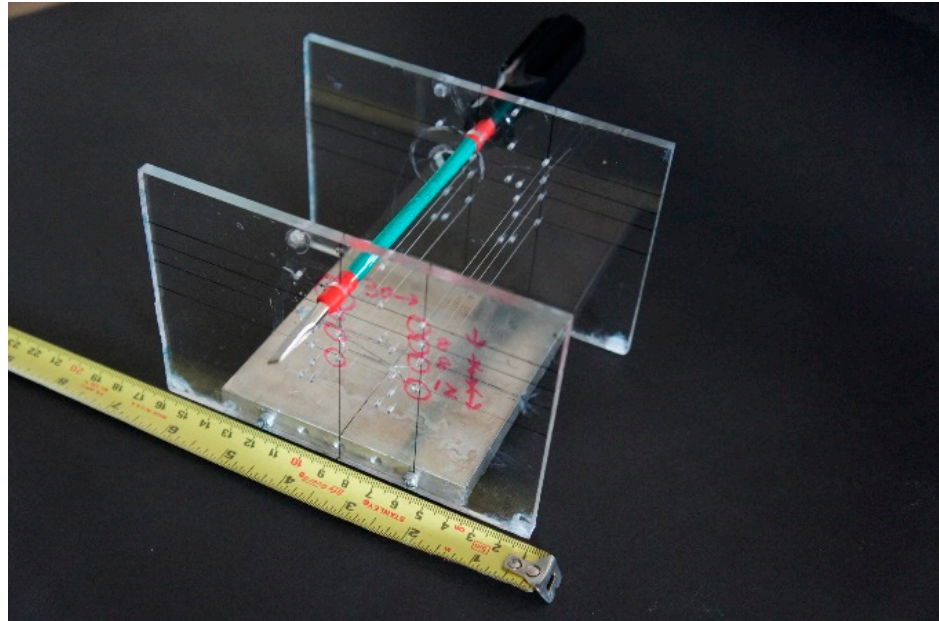
2. Experimental Setup

Obscuring by acoustic shadow in an ultrasound image is somewhat similar to the phenomenon of an eclipse, whereby one object to be imaged is shielded by the shadow of another. A forward model study is carried out to demonstrate the effects of acoustic shadowing on the ultrasound image.

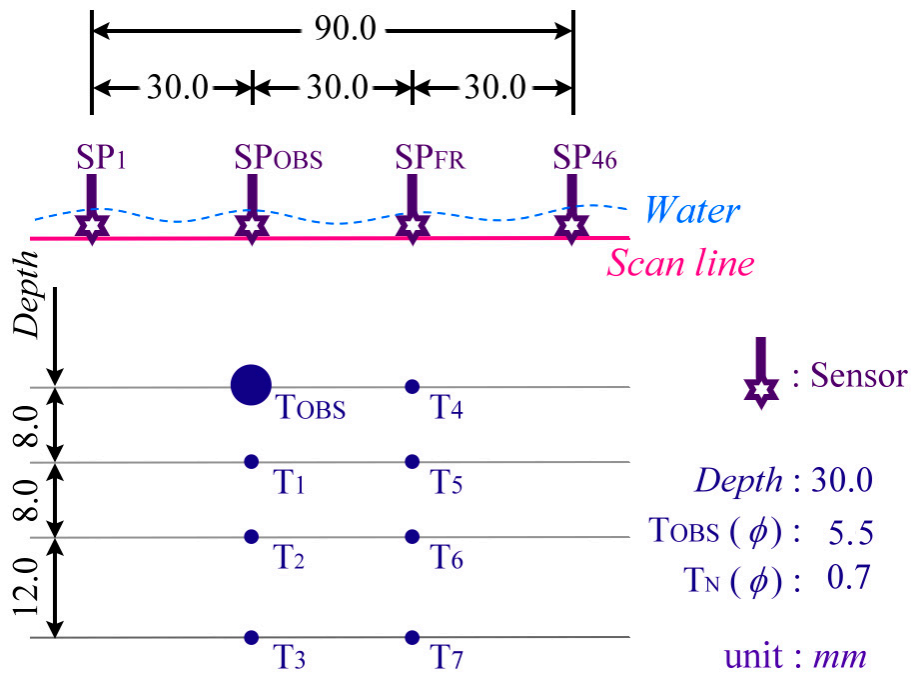
2.1. Physical Model

The physical model created to perform this shadowing scan consists of a skew driver rod and seven fishing lines (Figure 1a). The rod (T_{OBS}), 5.5 mm in diameter, is used as an obstacle for three fishing lines (T_1 , T_2 , and T_3). The other four fishing lines (T_4 , T_5 , T_6 , and T_7) are used to serve as a comparison. The diameter of the fishing line (T_N) is 0.7 mm. Taking gallstone ultrasound as an example, T_1 , T_2 , and T_3 can be considered to be small gallstones shadowed by a big one, T_{OBS} . To create the shadowing effect and, as a contrast, T_{OBS} , T_1 , T_2 , T_3 , T_4 , T_5 , T_6 , and T_7 , respectively, are aligned inline. For this purpose, T_1 , T_2 , and T_3 are positioned behind T_{OBS} to obtain a shadowed image for the scan position SP_{OBS} . Additionally, SP_{FR} , T_4 , T_5 , and T_7 are also aligned inline for an obstacle-free scan. Both

of the alignment lines are perpendicular to the scan surface (Figure 1b). The pink dot-line shown in Figure 1 indicates the scan line. SP_{OBS} and SP_{FR} located on the dot-line are two specific scan positions to perform shadowed and shadow-free scans.



(a)



(b)

Figure 1. (a) A picture of the created model. (b) Scales of the model and the relative positions of the targets to be scanned. Capital T stands for the target, and the scripts of OBS and the numbers denote the obstacle and the positions of different targets to be imaged. SP_{OBS} and SP_{FR} are two specific scan positions to perform obstacle and obstacle-free scans.

2.2. Laboratory Manipulation

For the process of data acquisition, the model is soaked into a water tank to perform an immersed scan (Figure 1b). The P-wave velocity in water is premeasured as 1450 m/s. The

active transducer used to facilitate our laboratory manipulation is an Olympus (V204-RM 2.25 MHz/6 mm) [18]. The dominant frequency of the active transducer thus makes the wavelength of the propagating P-wave 0.6 mm; hence, the dimensions of TOSB and TN are approximately ten times and equal to the dominant wavelength, respectively.

For the process of data acquisition, a PANAMETRICS 5058 pulser–receiver is adjusted to be either in single probe or a pulse/echo mode to perform a B-mode scan and a pitch/catch scan, generate an electric pulse, receive the electric signal, and synchronize (Sync) the digital oscilloscope (Tektronix DPO3034) [19,20]. The digitized radio frequency (RF) signal is then downloaded from the digital oscilloscope via a general-purpose interface bus (GPIB) and IEEE-488 communication to a personal computer for further processing. When the digitized echo signal is created, the transducer is automatically moved to the next location.

2.3. Restoration Algorithm-Synthetic Aperture Focusing Technique (SAFT)

In US, data are acquired simultaneously from all directions over a number of emissions. Echo signals are recorded independently by individual elements of the receive sub-aperture. However, signals shown in the ultrasound image may not indicate the real position of where the acquired echoes originated. To access reliable inside information of a medium from an ultrasound image, a restoration operation has often been applied to the acquired data to reconstruct the interior structure. Among all kinds of existing restoration algorithms, SAFT is the one that has been around for a long time and is extensively used to achieve echo energy refocusing and image resolution enhancement. In the process of SAFT, the relationship between the echo signals of N sensors disposed of inline (multi-channel scans) is calculated, and thereafter a defocused image is reconstructed by summing all demodulated input echo signals [21–25]. SAFT can be performed either in the image domain or the frequency domain to accommodate image reconstruction. In the subsequent stage of image processing in this work, SAFT is performed in the time domain using delay-and-sum (DAS) processing to restore ultrasonic images obtained from B- and pitch/catch scans under acoustic shadowing.

A brief description of applying SAFT to facilitate the reveal of a shadowed image is shown in Figure 2. It is assumed that a point diffractor (T) is immersed in water, and a sensor emitting a spherical wave is used to obtain a B-scan image of the diffractor (T) (Figure 2). By summing the delayed time traces of the B-scan image [$SP_i(x \pm I \times dx, t + dt_i)$], the reconstructed image [$SP(x, t)$] processed by the SAFT is given by

$$T = SP(x, t) = \sum_{i=-n}^n SP_i(x \pm i \times dx, t + dt_i), \quad (1)$$

$$dt_i = \sqrt{\left(\frac{2i \times dx}{V}\right)^2 + t^2} - t, \quad (2)$$

where dx is the successive lateral scanning interval; t is the vertical two-way propagation time of the pulse from the probe to the flaw and back; and V is the speed of sound in water. For scanning position x , dt_i in (1) is the time delay for the successive scanline, $i \times dx$, with respect to the point diffractor (T); $i = \pm n$; the maximum lateral distance at which the echo signals diffracted from the diffractor (T) can be detected by the sensor.

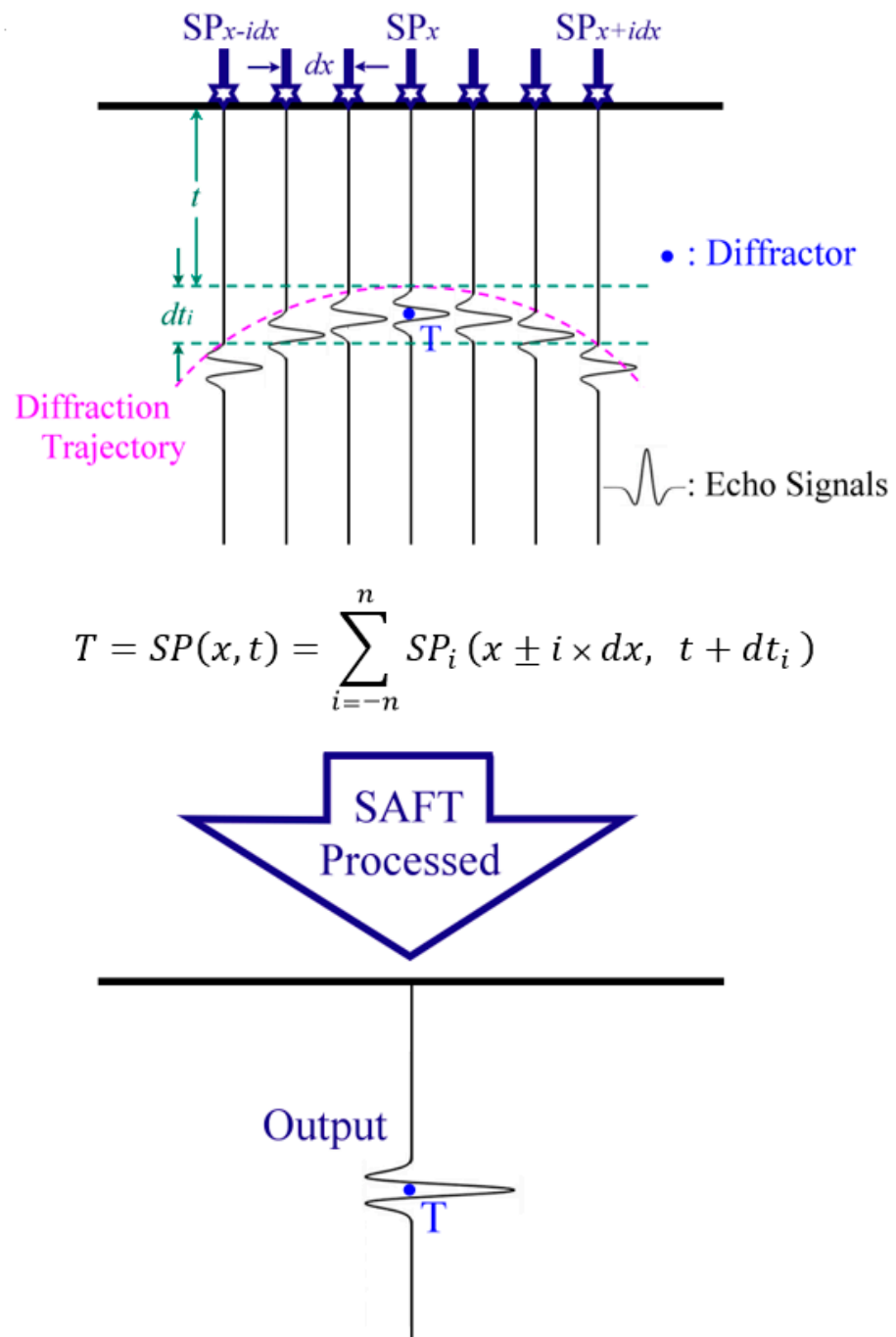


Figure 2. A brief description of the SAFT process.

3. Results

3.1. Synthetic Simulation

Taking the spreading attenuation into consideration, a synthetic profile of the pitch/catch scan obtained from the model is computed using the Levin equation [26]. At a sampling interval of 16 ns, a zero-phase Ricker wavelet is used to compute the synthetic profile using FORTRAN language. The velocity used is the same as the modeling material, i.e., 1450 m/s. Following the practical operation, the spacing interval of two successive traces is fixed at 2 mm. In the following paragraphs, the synthetic profile is used to assist image interpretation and serve as test data to evaluate the performance of SAFT in image restoration. Figure 3a shows the synthetic profile which is computed, based on the theoretical echo paths that respond from the “eight targets”, i.e., the relative positions of

T_{OBS} and T_N inside the created model. According to point diffraction theory, there should be eight hyperbolic trajectories showing up in the synthetic profiles, with the targets as the apexes. When the scan positions (SPs) move or are close to the projection of T_{OBS} , echo signals around the vicinity of the apexes T_1 , T_2 , and T_3 are purposely muted to simulate and demonstrate the shadowed images in an anechoic zone (Figure 3a). In the synthetic and the following images, echo signals are displayed using a linear grayscale from black (the smallest) to white (the largest).

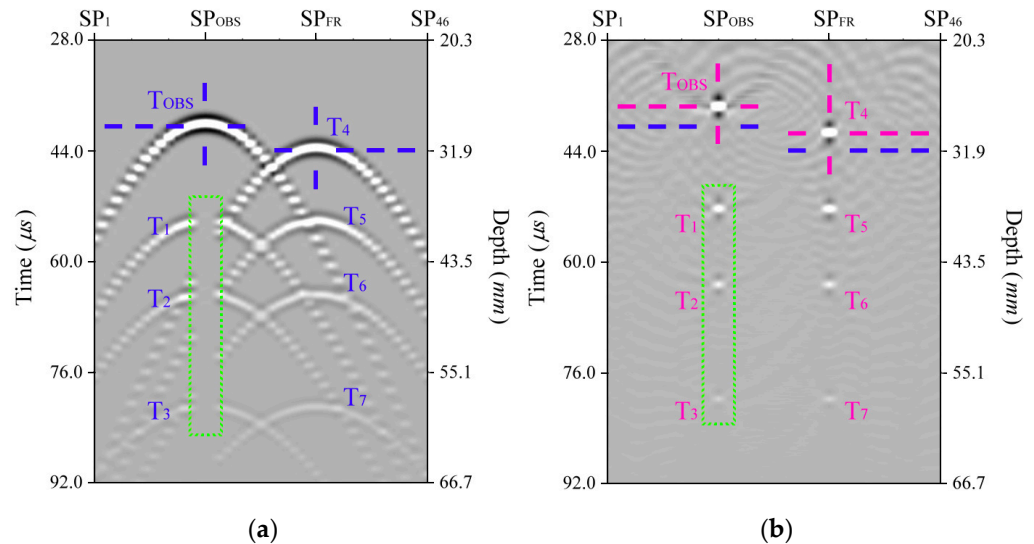


Figure 3. (a) A synthetic profile of the created model for a pitch/catch scan in the status of shadowed and shadow-free. Based on the theoretical echo paths, echoes that come from eight targets are individually shown as eight hyperbolic trajectories. The dotted rectangular line indicates an anechoic zone. (b) The output of the SAFT restoration from (a). The intersections of the dark-blue and pink cross shown in the figure stand for the theoretical imaged and restored positions of T_{OBS} .

The synthetic profile is SAFT-processed; Figure 3b shows the output images of restoration. Even though part of the echo signals is purposely muted in the incomplete trajectories, T_1 , T_2 , and T_3 respond to the acoustic shadow. All the hyperbolic trajectories shown in Figure 3a are successfully refocused as eight spots and repositioned in Figure 3b. The apex positions of T_{OBS} and T_4 that show up at $40.0 \mu\text{s}$ and $43.6 \mu\text{s}$ in Figure 3a are shifted upward to $37.6 \mu\text{s}$ and $41.3 \mu\text{s}$, respectively, in Figure 3b, in response to the SAFT process. In other words, the events of T_{OBS} and T_4 are not only successfully restored, but also relocated to a new position.

3.2. Experimental Results

To facilitate the objective of this study, the created model is scanned using B-mode and pitch/catch arrangements. For the pitch/catch mode scan, the spacing interval of two active transducers is fixed at 20 mm. The pink line shown in Figure 1 indicates the scan that runs perpendicular to the orientations of the rod of the skew driver and fishing lines. The scan line extends from 30 mm on the left-hand side of SP_{OBS} to 30 mm on the right-hand side of SP_{FR} (Figure 1b). Hence, the total length of the scan line is 90 mm. The offset interval in between each successive scan is 2 mm. In total, 46 observations are performed in a complete scan. Each observation consists of 2500 points sampled at an interval of 8 ns, which equates to a time frame of $20 \mu\text{s}$.

Figure 4a shows the result of the B-mode scan. Though the synthetic profile shown in Figure 3a is computed for the pitch/catch scan, it can still be used to assist in identifying images obtained from the B-mode scan (Figure 4a). Once a comparison is made between Figures 3a and 4a, it can be identified that their echo signals observed at $41.3 \mu\text{s}$ and $77.6 \mu\text{s}$ at SP_{OBS} in Figure 4a came from T_{OBS} and T_3 , though the echo strength is weak for T_3 . In

terms of the eclipse, T_1 , and T_2 , which fall within the umbra area and at the intersection of umbra and antumbra of the echo field caused by T_{OBS} , fail to be imaged. At SP_{FR} , fishing lines labeled T_4 , T_5 , T_6 , and T_7 are detected at $40.8 \mu s$, $48.7 \mu s$, $61.1 \mu s$, and $78.1 \mu s$. In addition, a question-marked event is observed at the lower center of Figure 4a, and is identified as a multiple-echo of T_{OBS} . Once the original observations (Figure 4a) are SAFT-processed, Figure 4b shows the output. In Figure 4b, the images of T_{OBS} , T_3 , T_4 , T_5 , T_6 , and T_7 are all well restored at the proper positions. The multiple echo, shown by a red question mark in Figure 4a, which comes from T_{OBS} , is gone.

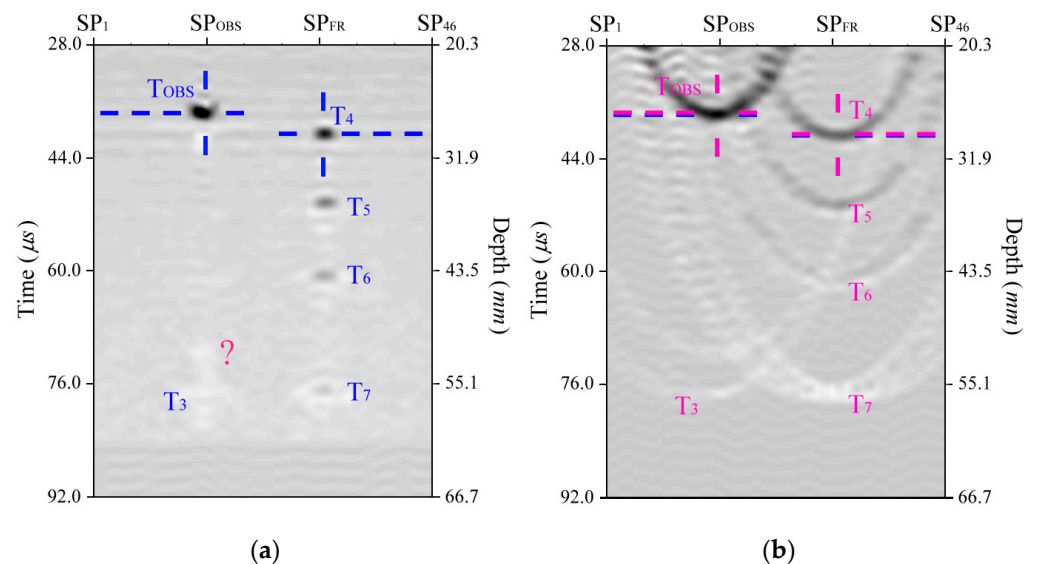


Figure 4. (a) Original B-mode scan data. Except for T_2 and T_3 , the other targets are all echo imaged. The intersection of the dark blue dashed lines indicates the image of T_{OBS} . A phantom echo which is question marked at the lower center position of SP_{OBS} is identified as a multiple of T_{OBS} . (b) Restored image of (a) which is processed by SAFT. All of the target images, except for T_2 and T_3 , are well restored. The intersections of the dark blue dashed lines and pink dashed lines show the position of T_{OBS} before and after the SAFT process.

Figure 5a shows the result of the pitch/catch scan. In Figure 5a, the echoes from T_{OBS} and T_3 are detected at $40.1 \mu s$ and $79.8 \mu s$ at SP_{OBS} , respectively. Out of T_{OBS} and T_3 , one more echo is detected at $63.3 \mu s$. Referring to the synthetic profile (Figure 3a), this new echo is identified as T_2 . In addition, echoes coming from T_4 , T_5 , T_6 , and T_7 are individually observed at $43.5 \mu s$, $53.5 \mu s$, $63.6 \mu s$, and $81.1 \mu s$ at SP_{FR} . However, limited by the overlap of the beam divergence angle, the trajectories of imaged targets show up as an incomplete hyperbolae in the acquired scan [27,28]. Thereafter, the original observations are SAFT-processed. Once again, the intersections of dark blue dashed lines and pink dashed lines indicate the original and SAFT-processed images of T_{OBS} and T_4 , respectively. In Figure 5b, it can be seen the original echo image shown in the raw data, i.e., Figure 5a, is not just restored but also properly repositioned.

To acquire more details into the performance of SAFT in shadowed image restoration, the acquired echo signals and SAFT-processed data are Hilbert-transformed to perform echo strength analysis [29]. The outputs of echo strength analysis are normalized using the maximum echo strength of the raw data and SAFT-processed events at the specific scan positions, i.e., SP_{OBS} . In Figure 6, the normalized echo strengths of observed echoes (raw data; in dark blue) and restored images (in pink) along the axial direction for the B-mode scan and pitch/catch mode scan are displayed. For the B-mode scan (Figure 6a), it can be seen that the observed events are refocused at the positions where the targets are imaged. For the pitch/catch scan (Figure 6b), the performance of the SAFT process in image restoration becomes more obvious. The images of the detected targets are not just refocused but also repositioned. Although the background noise comes with the restoration

process, the image resolution is enhanced. Detailed information of observed (raw) data and SAFT-processed data are tabularized in Tables 1 and 2, respectively.

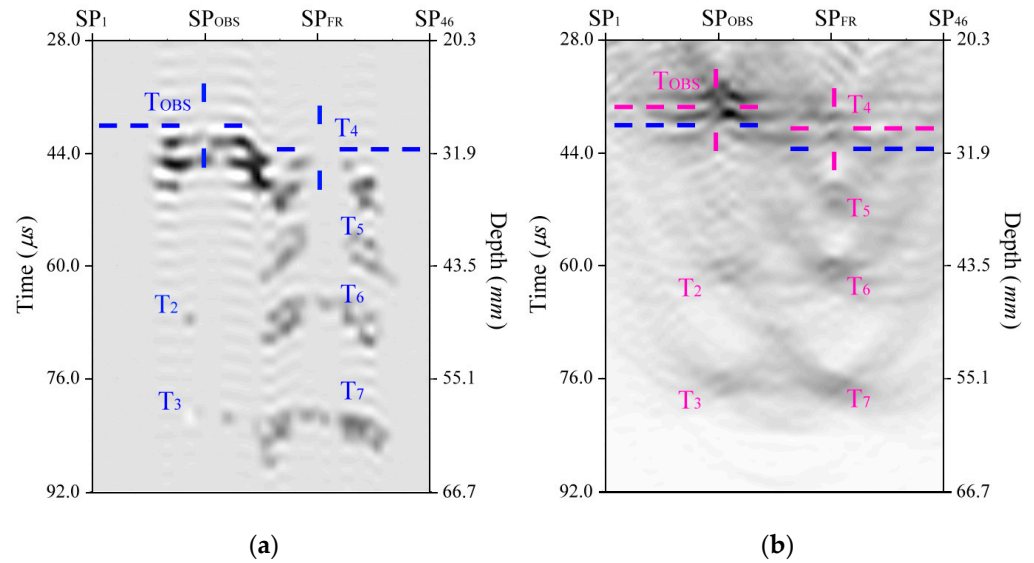


Figure 5. (a) Original pitch/catch scan data. Except for T₁, which is positioned too close to T_{OBS} and falls within the anechoic zone, echo signals from the other targets are all detected. (b) Restored image of (a) which is processed by SAFT. The performance of SAFT in image restoration can be shown by the upward shift of the dark blue dashed line to the pink dashed line.

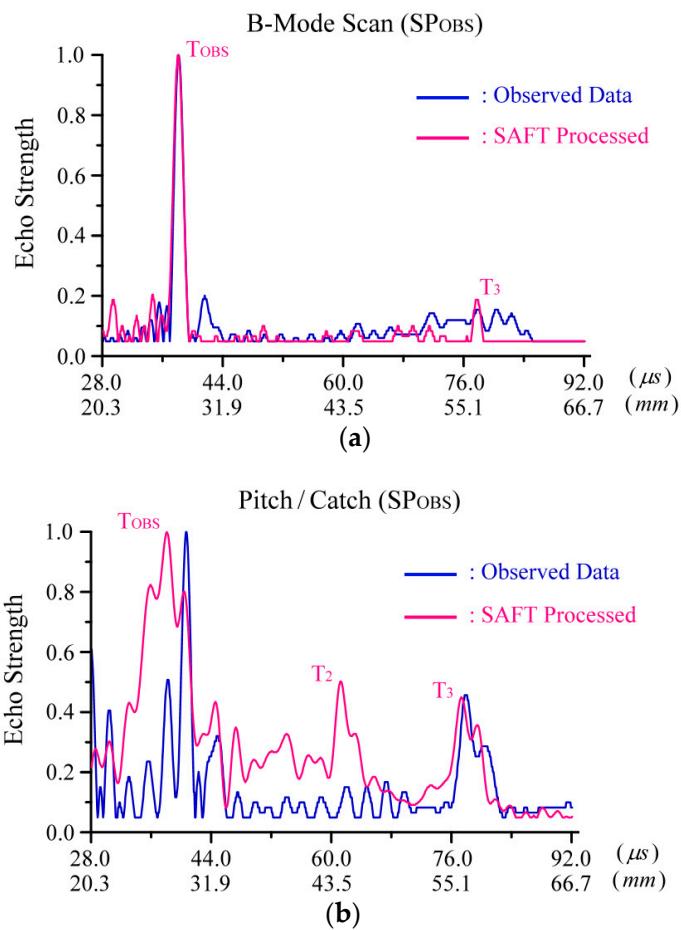


Figure 6. Echo strength analyses of (a) B-mode scan and (b) pitch/catch scan at SP_{OBS}. Through the processed noise with restoration, the resolutions of imaged targets are enhanced.

Table 1. Details of the original observations (raw data) and SAFT-processed data for the B-mode scan (Figure 3). Numbers shown below the targets (T_{OBS} and T_N) are the depths of the centers and the tops of the relative holes (center/top). Numbers above the slash of relative imaged echoes show the information of original observations and those below the slash are obtained from the results of the SAFT process.

B-Mode Scan			
SP_{OBS}		SP_{FR}	
T_{OBS} 30.0/27.25 (mm)	41.3/37.5 (μs) 27.5/27.2 (mm)	40.8/40.7 (μs) 29.6/29.5 (mm)	T_4 30.0/29.65 (mm)
T_1 38.0/37.65 (mm)		48.7/48.7 (μs) 36.8/36.8 (mm)	T_5 38.0/37.65 (mm)
T_2 46/45.65 (mm)		61.1/61.1 (μs) 44.3/44.3 (mm)	T_6 46/45.65 (mm)
T_3 58/57.65 (mm)	77.6/80.0 (μs) 56.3/58.0 (mm)	78.1/80.2 (μs) 56.7/58.1 (mm)	T_7 58/57.65 (mm)

Table 2. Details of the original observations (raw data) and SAFT-processed data for the pitch/catch mode scan (Figure 4). Numbers shown below the targets (T_{OBS} and T_N) are the depths of the centers and the tops of the relative holes (center/top). Numbers above the slash of relative imaged echoes show the information of original observations and those below the slash are obtained from the results of the SAFT process.

Pitch/Catch Scan			
SP_{OBS}		SP_{FR}	
T_{OBS} 30.0/27.25 (mm)	40.1/37.7 (μs) 29.1/27.3 (mm)	43.5/41.7 (μs) 31.6/30.2 (mm)	T_4 30.0/27.25 (mm)
T_1 38.0/37.65 (mm)		53.5/51.6 (μs) 38.8/37.4 (mm)	T_5 38.0/37.65 (mm)
T_2 46/45.65 (mm)	63.3/60.8 (μs) 46.1/44.1 (mm)	63.6/61.9 (μs) 46.1/44.9 (mm)	T_6 46/45.65 (mm)
T_3 58/57.65 (mm)	79.8/77.5 (μs) 57.8/56.2 (mm)	81.1/81.0 (μs) 5.8/58.8 (mm)	T_7 58/57.65 (mm)

4. Discussion

At present, there is no relevant research which explores the potential lesions lying in acoustic shadow; a differential diagnosis is the best that can be done [7,17]. This current research is the first use of SAFT to reveal the existence of an object that is in the acoustic shadow. In addition, to simulate human tissue, this study uses water as the medium and monofilament to perform immersed scans. The low acoustic impedance contrast between water and the monofilament line thus degrades the laboratory data. However, satisfying results are still being achieved, providing effective information for the future development of ultrasonic detection methods.

Before directly applying SAFT to the laboratory data, a synthetic pitch/catch scan profile is computed, based on point reflection/diffraction theory. Eight targets of different spatial positions are purposely arranged. In Figure 3a, the theoretical echo signals that can be detected from the created targets show up as eight hyperbolic trajectories. To simulate a shadowed image, part of the echo signals from three of the targets, i.e., T_1 , T_2 , and T_3 , are purposely silenced. Once the synthetic image is SAFT-processed, Figure 3b demonstrates the output. In Figure 3b, it can be seen that the original images of all created targets, T_{OBS} and T_N , are perfectly reconstructed and repositioned. Restoration is also expected for the shadowed targets. The technique requires a partial or distorted signal for the restoration algorithm to reliably reconstruct the shadowed object. In particular, a sufficient amount

of data is required to achieve a satisfactory restoration job. In other words, a degraded restoration of an image can be achieved as a result of incomplete echo signals.

In the immersed experiments, the created model is scanned by B-mode and then pitch/catch arrangements. For clarity, the theoretical echo paths for B-mode and pitch/catch scans are depicted and shown in Figure 7. In Figure 7a, we can see that when the scan is performed at SP_{OBS} , targets (T_1 , T_2 , and T_3) that are located behind the obstacle (T_{OBS}) might not be echoed and become invisible in the original scan. Once the scanning is performed away from SP_{OBS} , e.g., at SP_{FR} , the shadowed targets can be partly echoed. In the essence of image restoration, an original image is restored by calculating the relationship between the echo signals of N sensors disposed of inline (multi-channel scans) and summing up all demodulated echo signals detected (Figure 3).

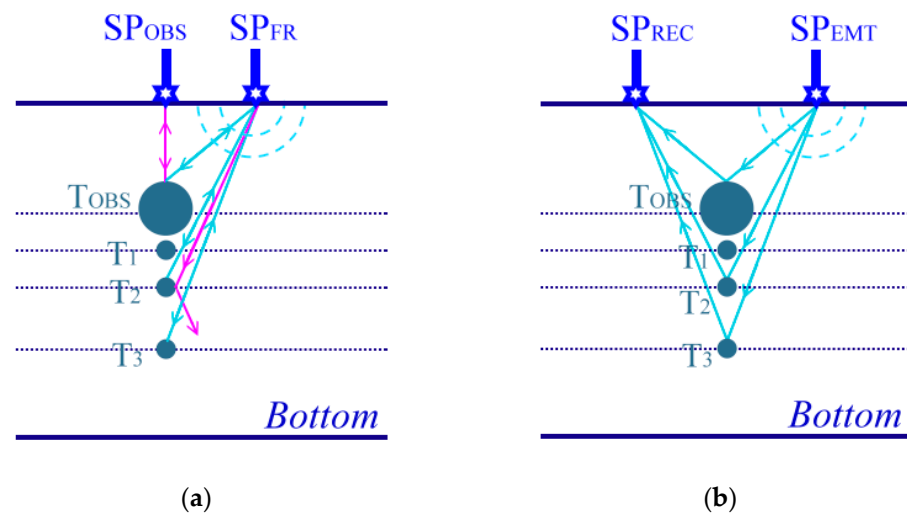


Figure 7. Schematic of (a) B-mode and (b) pitch/catch mode scans and the theoretical echo-paths for the active transceiver(s). SP stands for scan position, and subscripts OBS, FR, EMT, and REC are the obstacle, obstacle-free, emitter, and receiver, respectively.

In the practical operation of the SAFT process, the performance of image restoration is also highly dominated by the beam pattern, i.e., the divergence angle of the active sensor. The beam pattern is determined by factors such as the velocity of the medium to be scanned, the frequency and size of the active sensor, and the acoustic phase characteristics of the vibrating surface [27,28], possibly due to the effects of wavefront healing or whether the created model is scanned using B-mode or pitch/catch. The targets positioned behind T_4 , i.e., T_5 , T_6 , and T_7 , are all echoed in the scan images (Figures 4a and 5a) [30]. The radiation angle of an active sensor is proportional to the sound wave in the medium. In our immersed scan, the P-wave propagates with a slower velocity in water and limits the divergence angle of the active sensor. The limited divergence angle thus narrows the overlap of the emitted beam and reflected beam; therefore, the acquired trajectories originated by reflection/diffraction are incomplete (Figure 5a). Regardless of the scanning arrangements, target T_1 always fails to be echoed and restored. Our laboratory results thus show that image restoration cannot happen out of nothing. Once a target to be imaged falls within the anechoic zone, nothing can be done to restore the original image.

5. Conclusions

Medical diagnosis is only as good as the diagnostic tools used. In sonographic diagnosis, the US can only detect lesions from the anterior; it is rarely used to detect human soft tissue lesions in circumferential 360 degrees. The use of US could fail to provide reliable diagnoses of tumors located either between the heterotopic ossification and joint, or eyeball tumors, due to the skull barrier behind the eyeball, causing acoustic shadowing. Making use of a forward model study, the phenomena of acoustic shadowing were demon-

strated, and the digitized echo signals were obtained. Acquired data were processed by a restoration technique, i.e., SAFT. Restoration output commends a target that is imaged under acoustic shadowing could be conditionally revealed and encourages the feasibility of revealing the existence of a potential lesion behind the larger and harder tissues or lesions. However, there are some limitations. Unless a target to be imaged can be partly echoed in the multi-channel scans, a shadowed image will not be unveiled. In other words, only a shadowed lesion that can be echoed using ultrasonography could be diagnosed, which is theoretically reasonable. Once the targets of potential lesions are positioned in a totally anechoic area, i.e., umbra in eclipse, the scanning task will fail.

Author Contributions: Conceptualization, C.-H.C.; Data curation, J.-W.C.; Funding acquisition, K.-Y.H.; Methodology, C.-H.C. and Y.-F.C.; Project administration, K.-Y.H.; Software, Y.-F.C. and J.-W.L.; Writing—original draft, C.-H.C.; Writing—review & editing, K.-Y.H. All authors have read and agreed to the published version of the manuscript.

Funding: The research leading to this paper was financially supported by the Ministry of Science and Technology Taiwan under grant no. MOST 108-2314-B-006-048-MY2, MOST 109-2116-M-415-001-, and MOST 110-2314-B-006-020.

Acknowledgments: We wish to express our appreciation to anonymous reviewers for providing very constructive suggestions and comments in revising this paper. Our appreciation also goes to Richard Konopka and Grace Hsu for their valuable effort and time in editing this paper.

Conflicts of Interest: The authors declare no conflict of interest.

References

1. Kino, G.S. Acoustic Imaging for Nondestructive Evaluation. *Proc. IEEE* **1979**, *67*, 510–525. [CrossRef]
2. Ruiz-Reyes, N.; Vera-Candeas, P.; Curpia' án-Alonso, J.; Cuevas-Martí' nez, C.; Blanco-Claraco, J.L. High-resolution pursuit for detecting flaw echoes close to the material surface in ultrasonic NDT. *NDTE Int.* **2006**, *39*, 487–492. [CrossRef]
3. Robinson, T.M. Basic principles of ultrasound. In *Physics for Medical Imaging Applications*; Springer: Dordrecht, The Netherlands, 2007; Volume 240, pp. 101–110. ISBN 978-1-4020-5649-9.
4. Kremkau, F.W.; Taylor, K.J. Artifacts in ultrasound imaging. *J. Ultrasound Med.* **1986**, *5*, 227–237. [CrossRef]
5. Hu, R.; Singla, R.; Deeba, F.; Rohling, R.N. Acoustic Shadow Detection: Study and Statistics of B-Mode and Radiofrequency Data. *Ultrasound Med. Biol.* **2019**, *45*, 2248–2257. [CrossRef] [PubMed]
6. Dunmire, B.; Harper, J.D.; Cunitz, B.W.; Lee, F.C.; Hsi, R.; Liu, Z.; Bailey, M.R.; Sorensen, M.D. Use of the Acoustic Shadow Width to Determine Kidney Stone Size with Ultrasound. *J. Urol.* **2016**, *195*, 171–177. [CrossRef] [PubMed]
7. Zhou, Z.; Wu, S.; Chang, K.J.; Chen, W.R.; Chen, Y.S.; Kuo, W.H.; Lin, C.C.; Tsui, P.H. Classification of Benign and Malignant Breast Tumors in Ultrasound Images with Posterior Acoustic Shadowing Using Half-Contour Features. *J. Med. Biol. Eng.* **2015**, *35*, 178–187. [CrossRef]
8. Weinstein, S.P.; Conant, E.F.; Mies, C.; Acs, G.; Lee, S.; Sehgal, C. Posterior acoustic shadowing in benign breast lesions: Sonographic-pathologic correlation. *J. Ultrasound Med.* **2004**, *23*, 73–83. [CrossRef]
9. Raza, S.; Goldkamp, A.L.; Chikarmane, S.A.; Birdwell, R.L. US of breast masses categorized as BI-RADS 3, 4, and 5: Pictorial review of factors influencing clinical management. *Radiographics* **2010**, *30*, 1199–1213. [CrossRef]
10. Madabhushi, A.; Yang, P.; Rosen, M.; Weinstein, S. Distinguishing lesions from posterior acoustic shadowing in breast ultrasound via non-linear dimensionality reduction. In Proceedings of the 2006 International Conference of the IEEE Engineering in Medicine and Biology Society, New York, NY, USA, 30 August–3 September 2006; pp. 3070–3073.
11. Park, H.J.; Kim, K.B. Extracting acoustic shadowing from ultrasound image using local difference. *Indones. J. Electr. Eng. Comput. Sci.* **2019**, *13*, 205–209. [CrossRef]
12. Henderson, M.; Dolan, J. Challenges, solutions, and advances in ultrasound-guided regional anaesthesia. *BJA Educ.* **2016**, *16*, 374–380. [CrossRef]
13. Rani, S.; Jindal, S.; Kaur, B. A Brief Review on Image Restoration Techniques. *Int. J. Comput. Appl.* **2016**, *150*, 30–33. [CrossRef]
14. Abbas, R.F. Review on Some Methods used in Image Restoration. *Int. Multidiscip. Res. J.* **2020**, *10*, 13–16. [CrossRef]
15. Hoegh, K.; Khazanovich, L. Extended synthetic aperture focusing technique for ultrasonic imaging of concrete. *NDT E Int.* **2015**, *74*, 33–42. [CrossRef]
16. Hartzog, H.R. The NDT Technician: Multiple-Transducer Ultrasonic Techniques. *NDT Tech.* **2017**, *6*, 4.
17. Drukker, K.; Giger, M.L.; Mendelson, E.B. Computerized analysis of shadowing on breast ultrasound for improved lesion detection. *Med. Phys.* **2003**, *30*, 1833–1842. [CrossRef] [PubMed]
18. Ultrasonic Transducers. Available online: <https://sintrol.fi/wp-content/uploads/2019/10/Ultraaaniluotaimet.pdf> (accessed on 2 September 2022).

19. Model 5058PR High Voltage Pulser-Receiver. Available online: http://cdn-docs.av-iq.com/dataSheet/5058PR_Datasheet.pdf (accessed on 2 September 2022).
20. DPO3000 Series Digital Phosphor OscilloscopesZZZ. User Manual. Available online: https://www.csus.edu/indiv/t/tatror/eee_117_lab/3017_test_equipment/dpo3014%20user%20guide.pdf (accessed on 2 September 2022).
21. Busse, L.J.; Collins, H.D.; Doctor, S.R. *Review and Discussion of the Development of Synthetic Aperture Focusing Technique for Ultrasonic Testing (SAFT-UT)*; NUREGKR-3625; Pacific Northwest Lab.: Richland, WA, USA, 1984. [[CrossRef](#)]
22. Karaman, M.; Li, P.C.; O'Donnell, M. Synthetic aperture imaging for small scale systems. *IEEE Trans. Ultrason. Ferroelectr. Freq. Control.* **1995**, *42*, 429–442. [[CrossRef](#)]
23. Schmitz, V.; Chakhlov, S.; Müller, W. Experiences with synthetic aperture focusing in the field. *Ultrasonics* **2000**, *38*, 731–738. [[CrossRef](#)]
24. Jensen, J.A.; Nikolov, S.I. Synthetic aperture ultrasound imaging. *Ultrasonics* **2006**, *44*, e5–e15. [[CrossRef](#)]
25. Chang, C.H.; Chang, Y.F.; Ma, Y.; Shung, K.K. Reliable estimation of virtual source position for SAFT imaging. *IEEE Trans. Ultrason. Ferroelectr. Freq. Control.* **2013**, *60*, 356–363. [[CrossRef](#)]
26. Levin, F.K. Apparent velocity from dipping interface reflections. *Geophysics* **1971**, *36*, 467–618. [[CrossRef](#)]
27. Transducer Beam Spread. Available online: <https://www.nde-ed.org/NDETechniques/Ultrasonics/EquipmentTrans/beamspread.xhtml> (accessed on 31 August 2022).
28. Understanding How Frequency, Beam Patterns of Transducers, and Reflection Characteristics of Targets Affect the Performance of Ultrasonic Sensors. Available online: <https://www.massa.com/wp-content/uploads/2018/06/Massa-Whitepaper-3-DPM-160621.pdf> (accessed on 31 August 2022).
29. Bracewell, R.N. *The Fourier Transform and Its Application*; McGraw-Hill Book Co., Inc.: New York, NY, USA, 1986.
30. Hwang, Y.K.; Ritsema, J.; van Keken, P.E.; Goes, S.; Styles, E. Wavefront healing renders deep plumes seismically invisible. *Geophys. J. Int.* **2011**, *187*, 273–277. [[CrossRef](#)]